

# Li intercalation in 4 Å carbon nanotubes and related structures

Liu Hui-Jun

Key Laboratory of Artificial Micro- and Nano-structures of Ministry of Education and School of Physics and Technology, Wuhan University, Wuhan 430072, China

The unique one-dimensional structure and strong curvature effect of carbon nanotubes offer interesting channels for chemical doping. In this article, we summarize our recent density functional calculations on Li intercalation in three kinds of carbon nanotubes with a diameter of about 4 Å. We will discuss the structural, energetic, electronic and electrochemical properties of the intercalated systems. As these 4 Å nanotubes were originally fabricated inside the zeolite channels, our theoretical investigation is extended to the carbon nanotubes-zeolite complex. In addition, we will discuss Li doping in a related structure where the smaller (5, 0) tube is confined inside a larger (14, 0) tube to form a double-walled carbon nanotube. The theoretical calculations suggest that the 4 Å carbon nanotubes and related structures could be very promising candidates for Li-ion battery applications.

**Key words:** carbon nanotubes; Li intercalation; Li-ion battery; electronic properties; electrochemical properties; density functional calculations

CLC number : TM912.9 Document Code : A

## CONTENTS

I. Introduction	165
II. Computational details	166
III. Li intercalation in 4 Å SCNT	166
A. Interior doping	166
B. Exterior doping	168
IV. Li intercalation in carbon nanotube-zeolite complex	170
V. Li intercalation in DCNT	173
VI. Summary	175
Acknowledgments	175
References	175

## I. INTRODUCTION

The Li-ion rechargeable battery has been an attractive power source for its wide applications in the fields such as laptop computers, cellular telephones, and other electric vehicles. Usually the Li-ion battery is consists of metal oxides (such as  $\text{CoO}_2$  and  $\text{NiO}_2$ ) on the cathode side, and carbon materials with Li intercalated on the anode side in the charged state. Many types of carbon materials have been considered as the

anode of Li-ion battery, such as carbon black, coke, carbon fiber, graphite and so on. As a new member of the carbon materials family, carbon nanotube (CNT) has attracted a lot of attention from the science community since its discovery in 1991<sup>[1]</sup>, and the possibility to use CNTs as high performance Li-ion battery materials has been suggested.

A single-walled carbon nanotube (SCNT) can be viewed as a graphene sheet rolled into a cylinder and the structure usually has a helical arrangement of carbon hexagons. The diameter of a CNT is on the order of one nanometer and the length of it can be more than 1  $\mu\text{m}$ . Each nanotube can be characterized by a pair of integers ( $n$ ,  $m$ ), called helicity or chirality indices. Within the band-folding picture<sup>[2]</sup>, the electronic structure of carbon nanotubes is derived by a simple tight-binding calculation for the  $\pi$ -electron of carbon atoms. It is then predicted that a carbon nanotube can be either metallic or semiconducting, depending on whether or not  $n - m$  is an integer multiple of 3. The unique one-dimensional structure of carbon nanotube also offers an interesting channel for chemical doping. In particular, the Li doping in CNTs have been intensively investigated<sup>[3~23]</sup>. It was predicated that the bundle of nanotubes such as (10, 0) and (10, 10) have a high Li capacity<sup>[7]</sup>. The reversible Li storage capacity could increase to  $\text{LiC}_3$  when SCNT are chemically etched into short segments<sup>[10]</sup>. Due to the large specific surface area and strong curvature effect, small diameter carbon nanotubes may exhibit more interesting doping properties compared with large ones. Indeed, Udomvech *et al.* showed that small diameter nanotubes are at an advantage

Received date: 2011-11-16  
\*phlhj@whu.edu.cn

compared with large ones in Li-ion batteries<sup>[17]</sup>. In 2000, ultra-small SCNT have been successfully fabricated inside the confined environment of inert  $\text{AlPO}_4\text{-5}$  zeolite (AFI) channels<sup>[24]</sup>, and they were perfectly aligned with a diameter of about 4 Å, probably at or close to the theoretical limit. There are only three possible chiralities of these 4 Å tubes, namely, the zigzag (5, 0), the chiral (4, 2), and the armchair (3, 3), and all of them are known to co-exist inside the AFI channels<sup>[25,26]</sup>. These three types of tubes offer us a good opportunity to study the effect of chirality on the Li intercalation. Due to their ultra-small diameters, we have to go beyond the band-folding picture<sup>[2]</sup> to explain their physical and chemical properties.

In this article, we summarize our recent density functional calculations on Li intercalation in these SCNT. We shall see there are several possible sites for Li to be intercalated, including the interior and exterior of the nanotubes. The Li binding energies show strong chirality dependence and there is obvious charge transfer between the tube and the Li atom. The change of electronic structure induced by Li intercalation is studied and we find that a rigid-band picture offers a good description near the Fermi level. Moreover, the Li storage capacity can be reached to very high value which suggests that the 4 Å nanotubes could be promising candidates for the Li-ion battery anode. As these nanotubes were originally fabricated inside the AFI zeolite channels, our theoretical investigation is extended to the carbon nanotubes-zeolite complex which also exhibits higher Li capacity together with good cyclic stability during the charge and discharge process. A higher voltage can be obtained if the complex is used in a Li-ion battery. The third system we consider is also related to the 4 Å nanotubes where the smaller (5, 0) tube is confined inside a larger (14, 0) tube to form a double-walled carbon nanotube (DCNT). Although the 4 Å tube exists in a different chemical environment, our calculations indicate that the Li capacity of the system is still larger than the highest value of graphite intercalated compounds which may also find possible application in Li-ion battery.

## II. COMPUTATIONAL DETAILS

Our calculations have been performed using plane-wave pseudopotential formulation<sup>[27~29]</sup> as implemented in the Vienna *ab initio* simulation package (VASP). The exchange-correlation energy is in the form of Perdew-Wang-91<sup>[30]</sup> with generalized gradient corrections (GGA). We use ultra-soft pseudopotentials for all the atoms involved in the calculations. In the case of SCNT and DCNT, we adopt a standard supercell geometry so that the tubes are aligned in

a hexagonal array. The closest distance between the tube and its periodic images is set to 14 Å for SCNT and 24 Å for DCNT so that they can be treated as independent entities. The carbon nanotubes-zeolite complex is also modeled by using a supercell geometry so that the tubes are confined inside the AFI channels and arranged in a hexagonal array. Here we choose the zigzag (5, 0) as the prototype of the 4 Å nanotubes since its periodicity is almost perfectly commensurate with that of the AFI (one AFI elementary cell contains two zigzag (5, 0) unit cells). The  $\mathbf{k}$  points are sampled on a uniform grid along the tube axis for all the systems we considered. The cutoff energy is set to 286 eV for both the SCNT and DCNT, while it is larger for the carbon nanotubes-zeolite complex (394 eV). Optimal atomic positions are determined until the magnitude of the forces acting on all atoms is less than 0.05 eV/Å.

## III. LI INTERCALATION IN 4 Å SCNT

### A. Interior doping

As known, there are three types of SCNT that have diameters of about 4 Å, and they offer us a good opportunity to study the effect of chirality on the kinetics and energetics of the Li doping. We first focus on the interior doping. It had previously been shown<sup>[31]</sup> that doping Li into 5 Å tube (6, 0) to form a single-atom chain is favorable when the tube mouth is passivated by H. It is thus nature to ask whether Li atoms can penetrate the mouth of the 4 Å tubes with different chirality. To do so we use the so-called real space approach<sup>[31]</sup> where the tubes have finite length with nominal formulas  $\text{C}_{120}\text{H}_{10}$ ,  $\text{C}_{120}\text{H}_{12}$  and  $\text{C}_{108}\text{H}_{12}$  for the (5, 0), (3, 3) and (4, 2), respectively. All the carbon atoms at the mouth of the tubes are saturated by hydrogen atoms. In the calculation, two Li atoms are arranged to penetrate symmetrically, one on each end of the tube. The Li binding energies as a function of Li-Li distance measured from the geometric center of the tubes are shown in Fig. 1 where the (5, 0), (3, 3) and (4, 2) are marked by circles, triangles, and squares, respectively. The zero of the energy is defined as the total energy of a pristine tube plus free (spin-polarized) Li atoms. We see that the Li atoms have lower energy inside the tube than outside the tube, and the reaction is strongly exothermic relative to atomic Li. Moreover, there is no insertion barrier through the mouth of the tube. In all three cases, we find that the Li atoms prefer to sit along the axis once it is inside the tube. Since the Li atoms donate their 2s electrons to the carbon atoms and become positively charged, we would expect repulsive Li-Li interaction when the Li atoms are close together. However, the

screening of the tube is good so that the Li atoms do not feel the presence of each other until they are closer together than the screening length of the tube. The energy curve inside the tube is very smooth for (3, 3) and (4, 2), implying that there is essentially no diffusion barrier for Li inside. For the (5, 0) tube, the Li binds slightly stronger when it is facing the hexagonal rings than facing the zigzag bonds, leading to a small diffusion barrier of about 0.16 eV. These generic features of Li intercalation are rather similar to that of (6, 0) tube<sup>[31]</sup>.

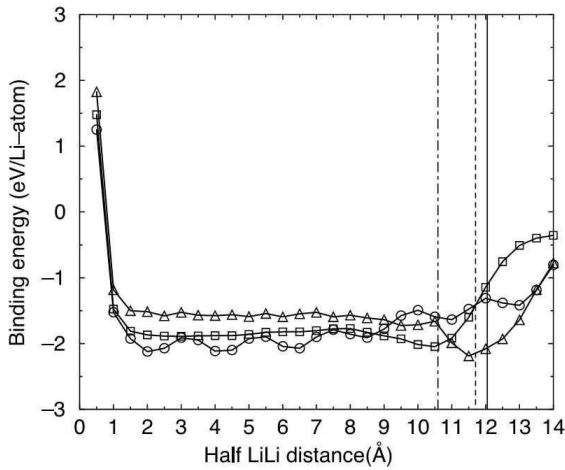


FIG. 1. Binding energy per Li atom as a function of the distance from the geometric center of the 4 Å SCNT of finite length. Circles: (5, 0) tube, squares: (4, 2) tube, and triangles: (3, 3) tube. The energy is calculated relative to atomic spin-polarized Li. The vertical lines mark the position of carbon atoms at the edge of each type of tube: solid line for (5, 0), dashed line for (3, 3), and dot-dashed line for (4, 2)

There are, however, some noticeable differences for Li intercalation between these three types of tubes. As noted already, the diffusion barrier is larger for (5, 0) than (4, 2) and (3, 3). We also see that once inside the tubes, Li binds much stronger with (5, 0) than (3, 3), with the chiral (4, 2) in between, indicating that there is a strong dependence of the binding energy on the chirality of these tubes. In addition, there is a local minimum for Li near the mouth of (3, 3) (marked by the dashed line in Fig. 1; while for (4, 2), the energy of the Li atom decreases monotonically as it approaches and penetrates the mouth (marked by the dot-dashed line). The Li binding energy for the (5, 0) tube is also decreasing from the outside to inside except for some position dependent variations. Summarizing the results, we find that certain features of the Li intercalation energetics do depend on the chirality of these tubes, even though the radius is nearly the same. Among the three chiralities, the Li atoms would preferably be doped into the (5, 0) and

(4, 2) tubes. One reason is that the energy is more favorable. Another reason is the existence of a local minimum near the mouth of the (3, 3) tube that may trap Li atoms.

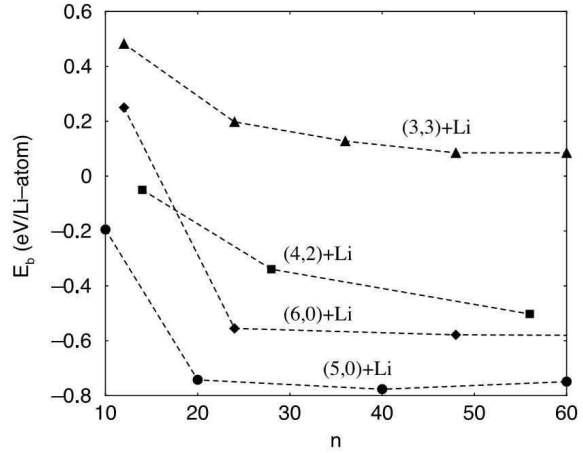


FIG. 2. Binding energy per Li atom as a function of the number of carbon atoms for one Li inside the 4 Å tubes (5, 0), (4, 2) and (3, 3), and 5 Å tube (6, 0). They are marked by circles, squares, triangles, and diamonds, respectively. The energy is calculated relative to bulk Li with bcc structure

The above real-space technique is efficient for considering the Li insertion with very small concentration. For higher Li concentration,  $\mathbf{k}$ -space method with periodic boundary condition is more suitable. We thus perform pseudopotential total energy calculations for these three tubes with Li concentration that ranges from  $C_{10}Li$  to  $C_{60}Li$ . For the results presented below, Li atoms reside on the tube axis, which has been explicitly checked and found to be the lowest energy position. The energy of the Li atoms depends slightly on their positions relative to the carbon rings. The lowest energy positions are found to be those facing the center of the hexagonal rings, and the energy is highest when the Li atoms are facing the zigzag bonds. We also find that the difference between the hexagonal site and zigzag site is very small for (3, 3) and (4, 2), and is about 0.17 eV for (5, 0), in good agreement with the real-space cluster calculations. Our results are shown in Fig. 2, where the binding energy is plotted against the number of carbon atoms per Li atom. The binding energy is defined as

$$E_b = E(LiC_n) - E(C_n) - E(Li_{bulk}) \quad (1)$$

where  $E(LiC_n)$  is the total energy of the tube containing Li atoms with a nominal formula of  $LiC_n$ ,  $E(C_n)$  is the total energy of the pristine tube, and  $E(Li_{bulk})$  is the total energy of Li in bulk structure (bcc). For comparison, the results for the 5 Å tube (6, 0) are also shown. This figure contains some interesting fea-

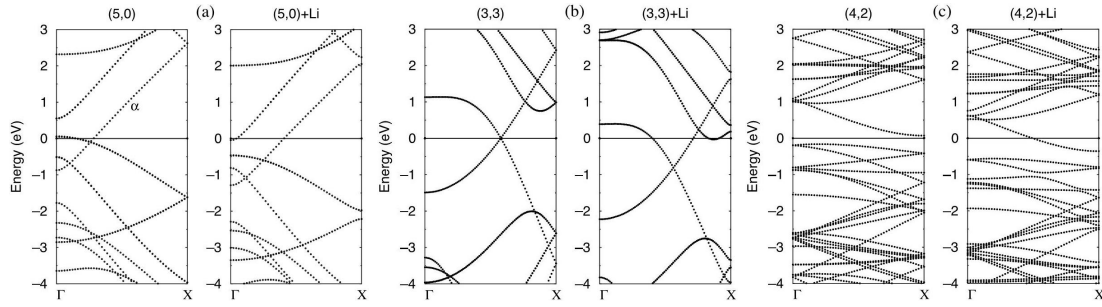


FIG. 3. Band structure for pristine and Li doped inside 4 Å tubes (a) (5, 0), (b) (3, 3) and (c) (4, 2). The Fermi level is at 0 eV

tures. We see that the binding energy of Li in the 4 Å tubes shows a marked dependence on chirality, with the order  $E_b(5,0) < E_b(4,2) < E_b(3,3)$ . Here, a more negative number means stronger binding and higher stability. The Li atoms tend to bind strongest with (5, 0) among the three possible chiralities. We note that the same order has also been found in the above real-space calculations with tubes of finite length. For Li in (5, 0) and (4, 2), the reaction is exothermic relative to bulk Li; while for (3, 3), the Li binding energy is positive, implying that the intercalation is unfavorable if the chemical potential of Li is set at that of bulk Li. When we compare (5, 0) with (6, 0) that has the same chirality but a bigger radius, we find that the binding of Li is stronger for the case of (5, 0). The energy curve for (5, 0) rises slower than that of (6, 0) when  $n$  is small (Li atoms are close together). This means that the screening is better in the case of (5, 0) than (6, 0). Both of these observations are consistent with the smaller radius of the (5, 0) tube.

Fig. 3 shows the band structures for Li doped (5, 0), (3, 3) and (4, 2), the unit cell of each tube contains 20, 12 and 56 carbon atoms, respectively. The band structure will depend on the Li concentration in the tubes, but the Li induced changes can be explained quite adequately by considering the concentration corresponding to one Li atom per unit cell, with nominal formulas  $C_{20}Li$ ,  $C_{12}Li$  and  $C_{56}Li$  for the (5, 0), (3, 3) and (4, 2) tubes, respectively. The band structures for the pristine tubes are also shown in Fig. 3 for comparison. We find that for all the cases we have considered, the rigid-band picture provides a good description near the Fermi level. The Fermi level of the nanotubes just get up-shifted as the carbon bands are filled by the 2s electrons of the Li atoms.

## B. Exterior doping

We now move to the discussions of exterior doping. Fig. 4 is a schematic ball-and-stick model of possible sites for Li atoms doped outside the 4 Å tubes. We see

there are three distinct doping sites for both the (5, 0) and (3, 3) tubes. The “bond1” site is associated with carbon-carbon bonds “along” tube axis while “bond2” is related to carbon-carbon bonds “around” tube circumference. The “center” site is facing the center of a hexagonal carbon ring. For the (4, 2) tube, there is an additional “bond3” site since it has three inequivalent carbon-carbon bonds. After geometry optimizations, we find that the distance between Li and the tube wall becomes 1.7 Å for the “center” site and 2.0 Å for the others, and chemical bonds are expected to be formed at such short distances. Table I gives the calculated Li binding energies for all the possible doping sites. We see that Li atom binds stronger with carbon-carbon bond “around” tube circumference than that “along” tube axis for all the three kinds of tubes. This is reasonable since the curvature effect weakens the  $\pi$  bonds wrapping around tube circumference and the Li atom is prone to reside there. For the “center” site, we find that (3, 3) tube has relatively larger distortion upon doping and the interaction between the tube and Li makes (3, 3) ellipse-like in shape. For the (5, 0) tube, the deformation is smaller and there is a slight increase of tube radius when Li is doped. In contrast, there is almost no change of the shape and diameter of the (4, 2) tube upon doping. Such difference is attributed to different doping concentration. Remember there are respectively 12, 20 and 56 carbon atoms per unit cell for the (3, 3), (5, 0) and (4, 2) tubes and each cell is doped with one Li atom. As can be seen from Table I, the “center” site has the lowest energy, which means that Li atom would preferably be doped into it among all the possible sites. The reason is that in the case of “bond” doping, Li will mainly donate its electron to the two nearest carbon atoms; while for the “center” doping, the nearest hexagonal carbon ring (six carbon atoms) will share the electron from Li.

As the “center” site is the most favorable in energy, we will focus on it in the following discussion. To make a better comparison between these three kinds of tubes, it is necessary to dope them with almost the

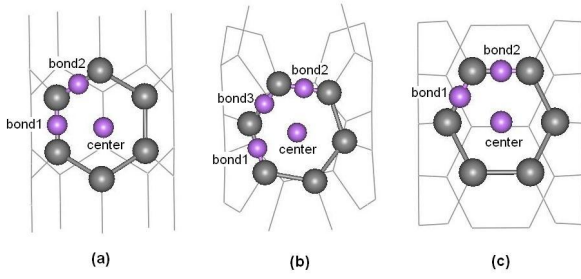


FIG. 4. Ball-and-stick model of possible sites for Li atom doped outside 4 Å carbon nanotubes: (a) (5, 0), (b) (4, 2) and (c) (3, 3)

TABLE I. Calculated binding energies (in unit of eV) for Li doped outside 4 Å tubes at different sites. The doped product has a nominal formula of  $C_{20}Li$ ,  $C_{56}Li$ , and  $C_{12}Li$  for (5, 0), (4, 2) and (3, 3) tubes, respectively.

tube	bond1	bond2	bond3	center
(5, 0)	-0.226	-0.419	/	-0.680
(4, 2)	-0.239	-0.275	-0.330	-0.532
(3, 3)	0.876	0.536	/	0.530

same concentration. This can be done by using a supercell containing 3 and 5 primitive cells for the (5, 0) and (3, 3) tubes, respectively. The resulting nominal formula is  $C_{60}Li$  which is very close to the case of (4, 2) tube ( $C_{56}Li$ ). At the new doping concentration, the calculated Li binding energies are listed in Table II. For comparison, the results for the interior doping are also given. We find that the exterior doping of Li is more favorable than the interior doping for all the three kinds of tubes. This is due to curvature effect which causes more charge outside the tube than that inside, and thus Li can bind more strongly on the outer surface. This fact is also consistent with the observation that the closest distance between tube and outside Li is shorter ( $\sim 1.7$  Å) compared with that of inside doping ( $\sim 2.0$  Å).

Remember that for the interior doping, the Li bind-

TABLE II. Calculated binding energies (in unit of eV) for Li doped outside 4 Å tubes at the “center” site. The doped product respectively has a nominal formula of  $C_{60}Li$ ,  $C_{56}Li$ , and  $C_{60}Li$ , for the (5, 0), (4, 2) and (3, 3) tubes, respectively. The results for inside doping are also given for comparison.

tube	inside	outside
(5, 0)	-0.74	-0.97
(4, 2)	-0.51	-0.53
(3, 3)	0.16	0.08

ing energy shows a strong chirality dependence, with the order of  $E_b(5, 0) < E_b(4, 2) < E_b(3, 3)$ . Note the chiral angle of each tube is 0, 19 and 30 degree, respectively. We see from Table II that the same trend is found for the exterior doping, that is, Li binds strongest with the zigzag (5, 0), weakest with the armchair (3, 3), and the chiral (4, 2) is in between. It is thus reasonable to conclude that such an order of binding energy is not a consequence of the precise positions or the chemical identity of the doped atoms, but rather an intrinsic property of the tube itself.

Fig. 5 shows the calculated energy band structure for Li doped outside the (5, 0), (3, 3) and (4, 2) tubes at the “center” site, with nominal formulas of  $C_{20}Li$ ,  $C_{12}Li$ , and  $C_{56}Li$ , respectively. The band structure is plotted with 50 uniform  $k$  points along tube axis. We first focus on the (5, 0) tube. Compared with the band structure of pristine tube<sup>[26]</sup>, we see from Fig. 5a that the Fermi level gets up-shifted as the Li atom denoting its 2s electron to the (5, 0) tube. Unlike the case of interior doping (Fig. 3a), the original degenerate bands are separated due to symmetry breaking when the Li atom is doped outside. In particular, the characteristic band crossing the Fermi level is now split because of band repulsion. As known<sup>[26]</sup>, an isolated (3, 3) tube has two linear bands symmetrically crossing the Fermi level which give rise to its desired metallic behavior. However, when Li is doped outside the (3, 3) tube, we see from Fig. 5b that the two linear bands are by no means symmetrical about the Fermi level, and there are significant changes of the band structure. This is also consistent with the fact that the (3, 3) tube becomes elliptical upon doping, as we mentioned above. As known<sup>[26]</sup>, (4, 2) tube is the only semiconductor in these three tubes and there is a small indirect band gap of about 0.2 eV. When Li is doped outside the (4, 2) tube, we find that the Fermi level moves up to cross a conduction band, making it metallic (see Fig. 5c). The change of the band structure follows a rigid-band picture, as mentioned above for the interior doping.

To study the charge transfer between the Li atom and these 4 Å nanotubes, we have plotted the differential charge density contours for the exterior doping at “center” site. The differential charge density is calculated using the expression

$$\Delta\rho = \rho(\text{tube} + \text{Li}) - \rho(\text{tube}) - \rho(\text{Li}) \quad (2)$$

Here  $\rho(\text{tube} + \text{Li})$  is the charge density of optimized tube with Li doped outside,  $\rho(\text{tube})$  and  $\rho(\text{Li})$  are those for the pristine tube and Li, respectively. Fig. 6 shows the calculated contour plot for the (5, 0) tube with one Li atom doped outside. It is obvious that there is charge accumulation around the neighboring carbon atoms and little is remain at the Li position.

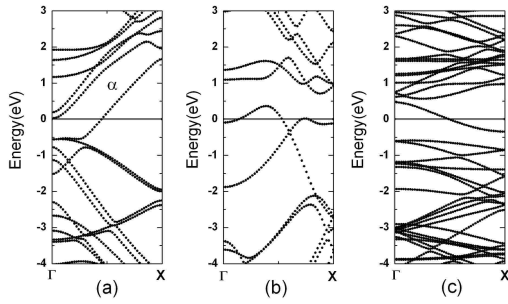


FIG. 5. Band structures for Li doped outside 4 Å tubes: (a) (5, 0), (b) (3, 3), and (c) (4, 2), with a nominal composition of  $C_{20}Li$ ,  $C_{12}Li$ , and  $C_{56}Li$ , respectively. The Fermi level is at 0 eV

This suggests that the Li atom donate its electron to the tube and a strong chemical bond is expected to be formed between them. Furthermore, there is a charge redistribution of the whole tube upon Li doping. This is probably a consequence of the existence of big  $\pi$  orbits on the tube surface and the electrons can move in these orbits. As the carbon atoms are farther away from the Li atom, such effect becomes weaker.

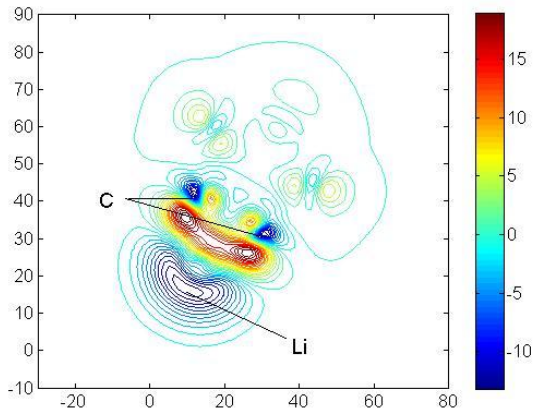


FIG. 6. Differential charge density contour on a plane perpendicular to the tube axis for Li doped outside the (5, 0) tube at the "center" site

As there are many equivalent positions of the "center" site for the outside doping, it is anticipated that the Li atoms can be doped with a large amount. Here we consider only the zigzag (5, 0) since the energy is the most favorable among the 4 Å tubes. As known, (5, 0) tube belongs to  $D_{5d}$  group and each unit cell has ten "center" sites arranged in two layers. We have calculated the binding energies for a series of Li concentration that ranges from  $C_{20}Li$  to  $C_{20}Li_{10}$ , and the results are shown in Fig. 7. At the doping concentration of  $C_{20}Li_{10}$ , we find the energy is positive which

means that it is not favorable for all the "center" sites to be occupied by Li atoms. The maximum exterior doping concentration is found to be  $C_{20}Li_7$ . In addition, one more Li atom can be intercalated into the interior of the (5, 0) tube, and the resulting binding energy is  $-0.019$  eV/Li-atom. Thus the highest Li storage capacity can be reached to  $C_{20}Li_8$ , or  $LiC_{2.5}$ , which is significant higher than that of graphite interaction compounds ( $LiC_6$ ). The enhanced Li capacity suggests that (5, 0) tube will be of potential applications in Li-ion battery.

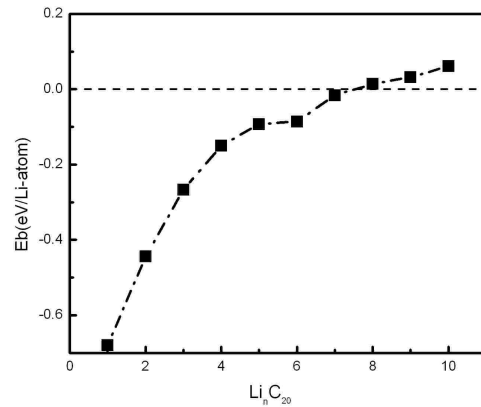


FIG. 7. Binding energy per Li atom as a function of Li concentration for exterior doping of the (5, 0) tube at the "center" site

#### IV. LI INTERCALATION IN CARBON NANOTUBE-ZEOLITE COMPLEX

As the 4 Å SCNT were originally fabricated inside the AFI zeolite template, in this section, we will consider the Li intercalation in a complex system where the 4 Å tubes are confined inside the AFI channels. AFI is a type of porous aluminophosphate single crystal<sup>[32]</sup>. Its framework consists of regularly alternating tetrahedral  $(AlO_4)^-$  and  $(PO_4)^+$  which form open one-dimensional channels packed in the hexagonal structure. The unit cell contains 112 atoms ( $Al_{12}P_{12}O_{48}$ ) with lattice constant  $a = 13.74$  Å and  $c = 8.47$  Å. Fig. 8 is a ball-and-stick model of (5, 0) tube confined inside the AFI channel, and the combined structure has a nominal formula  $C_{40}Al_{12}P_{12}O_{48}$ . For the freestanding (5, 0) tube, the Li can be doped both inside (site A) and outside the tube (site B). When the AFI is included explicitly, there are two additional sites (C and D) for Li to be intercalated. It should be mentioned that each one may have many equivalent sites in the hexagonal unit cell.

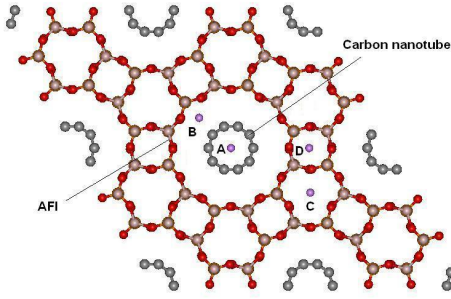


FIG. 8. Possible doping sites for Li doped in the carbon nanotube-zeolite complex

TABLE III. Calculated Li binding energies and volume changes for different doping sites in the carbon nanotube-zeolite complex with nominal formula of  $\text{LiC}_{40}\text{Al}_{12}\text{P}_{12}\text{O}_{48}$ .

doping sites	binding energies (eV/Li)	volume changes
A	-0.64	-0.5%
B	-1.31	0.07%
C	-1.06	-1.1%
D	-0.77	-1.8%

We first consider the low concentration limit such that there is only one Li atom per unit cell. Table III summarizes the calculated Li binding energies and volume changes for the above-mentioned doping sites. The definition of binding energy is similar to that of Li-doped SCNT discussed in Section III. The volume change percentage is given by the expression:

$$\alpha = \frac{V - V_0}{V_0} \quad (3)$$

Here  $V_0$  and  $V$  are total volume of the complex system before and after Li is doped, respectively. As can be seen from Table III, all the calculated binding energies are negative which means that the reactions are exothermic if the chemical potential of Li is set at that of bulk Li. Among all the four configurations, site B has the lowest energy and site A the highest with a difference of 0.67 eV. This value is significantly larger than that found for the outside and inside doping of freestanding (5, 0) tube. The reason is that the presence of AFI will enhance Li binding at site B. It was previously found that bare AFI is not favorable for Li doping<sup>[33]</sup>. However, when the tube is incorporated into the AFI channel, we see from Table III that even site C and site D are energetically favorable. Again, this suggests that the combination of carbon nanotube and AFI zeolite could be used to enhance Li binding. On the other hand, we see from Table III there are only slight changes of the cell volume upon

Li doping at all the four sites. In particular, Li at the most energetically favorable site B leads to a very small expansion of the volume. As there are many equivalent positions for site B between the outer wall of tube and the inner wall of AFI, it is reasonable to expect that Li can be doped with a large amount without significantly destroying the nanotube-zeolite structure.

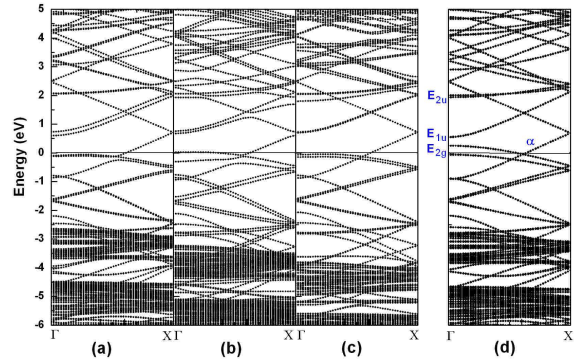


FIG. 9. Energy band structures of (a) the nanotube-zeolite complex with Li doped at site A, (b) the complex with Li doped at site B, and (c) the complex with Li doped at site C, (d) the un-doped complex. For each doping case, there is one Li per unit cell. The Fermi levels are at 0 eV

Fig. 9 shows the calculated energy band structures for the nanotube-zeolite complex with Li doped at different sites. For comparison, the band structure of pristine complex with the same unit cell is also shown. As AFI is an insulator with large gap, the energy bands around the Fermi level mainly come from the nanotube. Without Li, we see from Fig. 9d that the complex is metallic, as characterized by the down-shift of the band in the (5, 0) tube. The upper valence bands of the zeolite have little or no dispersions and are mainly located in two energy regions from -6.53 to -4.86 eV and -3.98 to -2.85 eV<sup>[34]</sup>. Upon doping of Li, we see from Fig. 9a~9c that the band structures follow roughly a rigid band picture. However, there are obvious band-splittings due to the symmetry breaking when the Li atom is intercalated into different sites. For example, the doubly-degenerate  $E_{1u}$  and  $E_{2u}$  bands in Fig. 9d are now separated by small gaps in Fig. 9a and 9c for the inside (site A) and hexagonal doping (site C), respectively. Such band-splittings are more obvious in Fig. 9b since the Li atom at site B results in a serious symmetry breaking. It is interesting to see that the separated  $E_{2g}$  bands in Fig. 9d tend to degenerate again for the Li doping at site A and C. On the other hand, the Li doping also changes the positions of the AFI's bands. In particular, the upper valence bands of AFI in Fig. 9c are down-shifted by

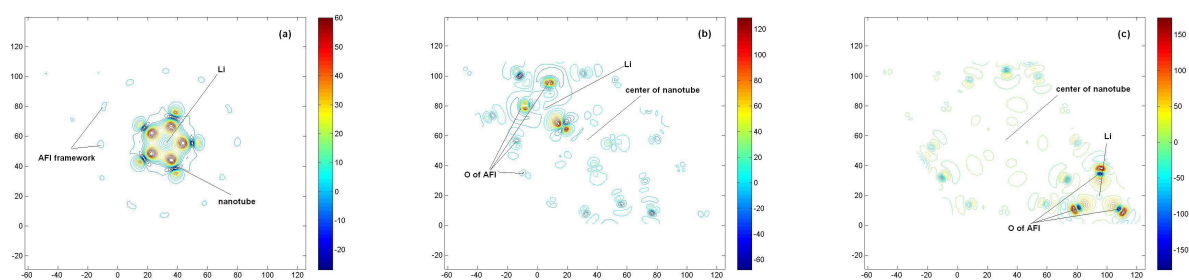


FIG. 10. Differential charge density contours on the (001) plane for Li doping at (a) site A, (b) site B, (c) site C

about 1.1 eV. In contrast, there is almost no shift for the AFI's bands in Fig. 9a. While for Fig. 9b, the change of the AFI bands is between these two cases. Such difference is probably due to the fact that at site A and C, the 2s electrons of Li are respectively transferred to the nanotube and AFI; while at site B, the electrons are given to both of them. The charge transfer can be clearly visualized by investigation of the differential charge density contours and Fig. 10a shows the differential charge density contour on the (001) planes for the case of inside doping at site A. We see that almost all the 2s electrons of the Li atom are donated to the carbon wall. When the Li atom is doped in the hexagonal center of AFI (site C), we see from Fig. 10c that the charge is mainly transferred to the three nearest O atoms of the AFI framework. For the doping at site B, however, the charge is transferred to both the carbon nanotube and AFI as can be seen from Fig. 10b. This is consistent with the fact that site B has the lowest energy among all the four configurations.

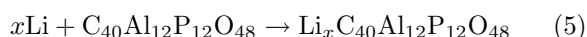
We now consider the high concentration limit. It is previously reported that an exothermic doping with 36 Li per unit cell of carbon nanotube-zeolite complex can be reached<sup>[33]</sup>. However, we checked that such higher doping concentration causes a volume expansion larger than 10%. Moreover, the AFI framework structure is destroyed and the nanotube has a serious distortion. It is generally accepted that for the anode materials used in Li-ion battery, the volume change should be less than 5% after Li intercalation. Otherwise, the stability and safety will become a serious problem. To get a maximum intercalation capacity, we should therefore insert Li atoms as more as possible and keep the volume change within 5% at the same time. As we mentioned before, there are many equivalent positions for the four possible doping sites. In our calculations, 24 Li atoms per unit cell are evenly arranged into four alternate layers between the outer wall of nanotube and the inner wall of AFI (site B). Additionally, two Li are inserted into the center of nanotube (site A) and one to each hexagonal

interstice (site C). The obtained configuration contains 28 Li atoms per unit cell with nominal formula of  $\text{Li}_{28}\text{C}_{40}\text{Al}_{12}\text{P}_{12}\text{O}_{48}$ , and the Li/C ratio is significantly larger than that obtained in the graphite intercalated compounds ( $\text{LiC}_6$ ). The corresponding Li binding energy is found to be  $-0.3$  eV which means that the intercalation is still favorable at such high concentration. On the other hand, there is only a small deformation of the AFI and tube's structure (Fig. 11a) and the volume expansion is found to be 4.7%. To see if such intercalation is reversible, we have done addition calculation where the 28 Li atoms are removed from the unit cell. It is interesting to find that after relaxation, the system recover to the original un-doped structure (Fig. 11b). This suggests that the carbon nanotube-zeolite complex may have good cyclic stability when used as the anode material of Li-ion battery.

To examine the electrochemical properties, we have calculated the Li-ion intercalation capacity by using the expression:

$$C_0 = 26.8 \times n \times m_0 / M \quad (4)$$

Here  $n$  is the moles of the transferred electrons.  $m_0$  and  $M$  are respectively the mass and atomic mass of the active matter. For our complex system with 28 Li atoms per unit cell, the calculated  $C_0$  is 386 mAh/g which is higher than the upper limit of graphite (372 mAh/g). As known, the Li-ion battery is often described as a rocking chair battery and Li moves in and out of anode and cathode during charge and discharge process. For the graphite intercalated compounds, the average voltage of  $\text{LiC}_6/\text{NiO}_2$  battery is 3.05 volt in calculation comparing with the experimental value 3.57 volt<sup>[35]</sup>. Here we can estimate the voltage value if the complex is instead used as anode material. The average voltage of the complex relative to bulk Li can be calculated as follows. During the intercalation process, we have:



The average voltage ( $E^{av,T}$ ) depends on the change of

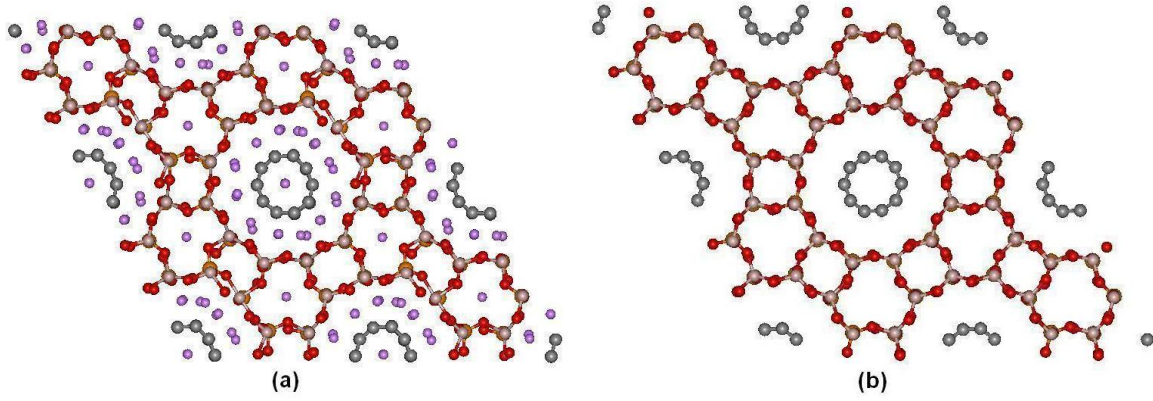


FIG. 11. The optimized structures of (a) the nanotube-zeolite complex doped with 28 Li atoms per unit cell, and (b) the relaxed structure when the 28 Li atoms are removed from the system

Gibbs energy ( $\Delta G^T$ ) in the reaction and can be given by<sup>[36]</sup>:

$$E^{av,T} = -\Delta G^T / nF \quad (6)$$

Where  $T$  denotes the absolute temperature,  $n$  is the moles of transferred electrons and  $F$  is the Faraday constant. Usually the temperature effect is very small in the calculation of the average voltage and can be neglected. On the other hand, the change of Gibbs energy can be approximately written as<sup>[37]</sup>:

$$\Delta G = \Delta E + P\Delta V - T\Delta S \quad (7)$$

where the 2<sup>nd</sup> term is of about  $10^{-5}$  eV/Li and can be neglected compared with the 1<sup>st</sup> term. The 3<sup>rd</sup> term vanishes at zero temperature. The average voltage is thus expressed as:

$$E^{av} = -\Delta E / nF \quad (8)$$

For the minimum ( $x = 1$ ) and maximum ( $x = 28$ ) doping, the calculated average voltage are 0.05 and 0.01 volt, respectively. The most popular cathode materials are  $\text{CoO}_2$  and  $\text{NiO}_2$  and they have a voltage of about 4 volt relative to bulk Li. Thus these small values suggest that the average voltage can be reached to about 4 volt if the nanotube-zeolite complex is used as anode material and the cathode is the conventional  $\text{CoO}_2$  or  $\text{NiO}_2$ .

## V. LI INTERCALATION IN DCNT

We now consider another complex system where the smaller (5, 0) tube is confined inside a larger (14, 0) tube to form a DCNT. The unit cell contains 76 carbon atoms where 20 come from the inner (5, 0) tube and 56 from the outer (14, 0) tube. Fig. 12 schematically shows possible Li doping sites in the DCNT. In

addition to the interior of the (5, 0) tube (site A), the Li atom can be also intercalated into the area between the inner wall and outer wall (site B). It is also possible for Li to be doped outside the (14, 0) tube (site C). Note that each site may have many equivalent positions. We begin our investigation with one Li atom per unit cell. For all the three configurations, we found that the DCNT keeps a very stable structure upon Li doping, and there is almost no change of the tube radius. Table IV summarizes the calculated Li binding energies for the three doping sites in the DCNT. For comparison, the results for the individual (5, 0) and (14, 0) tubes are also given. For the individual SCNT, we see from Table IV that the Li atom would like to be doped into the interior of the smaller (5, 0) tube rather than that of the larger (14, 0) tube. This is also the case for the outside doping in (5, 0) and (14, 0) tubes. As for the DCNT, we see from Table IV that two of them are energetically favorable. The one with the lowest energy is site B which can also be visualized as the outside of the (5, 0) tube or the inside of the (14, 0) tube. It should be noted that this energy value is significantly lower than those found at the corresponding sites of individual (5, 0) and (14, 0) tubes. This is reasonable since at the intertube space, the Li binds to both the inner and outer walls of the DCNT, while only one wall is involved for the case of individual tubes. It is interesting to find that the interior of the DCNT has a higher binding energy than that of the (5, 0) tube, while the exterior of the DCNT has a lower one than that of the (14, 0) tube. This is probably due to small charge transfer from the outer shell to the inner shell<sup>[38]</sup>. Indeed, we have done additional calculation which shows that for the un-doped DCNT about 0.29% of the electrons of (14, 0) tube are given to the (5, 0) tube. The transferred electrons will enhance the Li binding to the outer wall while reduce it to the inner one.

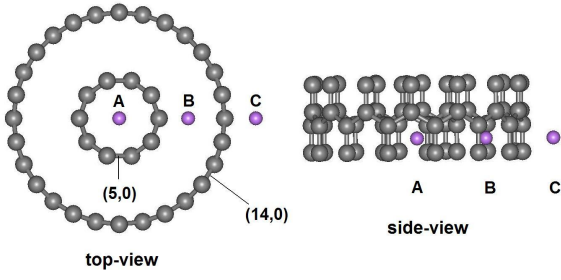


FIG. 12. Top and side view of possible Li doping sites in the DCNT (5, 0)@(14, 0). Note each site may have many equivalent positions

TABLE IV. Calculated Li binding energies (in unit of eV) for three different doping sites in the DCNT (5, 0)@(14, 0) with nominal formula of  $C_{76}Li$ . The calculated results for individual (5, 0) and (14, 0) tubes are also given for comparison.

sites	DCNT (5, 0)@(14, 0)	SCNT (5, 0)	SCNT (14, 0)
A	-0.67	-0.74	0.58
B	-0.96	/	/
C	0.29	-0.68	0.59

Fig. 13 shows the calculated energy band structures for the DWNT with Li-doped at different sites. Note there is only one Li atom per unit cell with the nominal formula of  $C_{76}Li$ . For comparison, the result of the pristine DCNT is also given. As the outer (14, 0) tube is semiconducting while the inner (5, 0) tube is metallic, we see from Fig. 13d that the un-doped DCNT is metallic and those bands from the (5, 0) tube (marked as red curves) and the (14, 0) tube can still be identified. However, some degenerate bands are now separated due to symmetry breaking caused by tube-tube interaction. Upon doping of Li, we see from Fig. 13a~13c that the overall topology of the band structure roughly follows a rigid band picture. Besides, the Li doping may change the relative position and/or degeneracy of those bands coming from the (5, 0) and (14, 0) tubes. When Li is introduced inside the inner tube (site A), we see from Fig. 13a that there is almost no change of the outer (14, 0) tube's bands. However, almost all the bands of the inner (5, 0) tube are pushed down by about 0.35 eV. The doubly-degenerate  $E_{1u}$  bands even get down-shifted by 0.60 eV and become lower than the upper valence band of the (14, 0) tube. The  $E_{2u}$  bands now coincide with the conduction band of (14, 0) tube at about 1.95 eV. For the intertube doping (site B), the change of (5, 0) tube's bands is similar to the case of site A except that the degenerate  $E_{2u}$  bands are now separated by a small gap of 0.18 eV. On the other hand, the bands of (14, 0) tube get down-shifted by about

0.58 eV and the original degenerate bands at about 1.50 eV are now separated. In particular, we observe obvious band-splitting due to strong band-band repulsion, as indicated by the small blue arrows in Fig. 13b. For the Li doping at site C, we see that the bands of (5, 0) tube are nearly the same as those found in the un-doped DCNT except that the  $E_{2g}$  bands are down-shifted a little bit; while the change of the bands from (14, 0) tube is similar to the case of intertube doping. The difference between Fig. 13a, 13b and 13c is due to the fact that when the Li atom is doped at site A and C, its 2s electrons are mainly transferred to the inner (5, 0) and outer (14, 0) tubes, respectively; while at site B, the electrons are donated to both of them. To have a quantitative understanding, we have performed Bader charge analysis<sup>[39~41]</sup> for the three doping configurations (Table V). We see that for interior doping, almost all the 2s electron (96%) of Li is transferred to the inner (5, 0) tube. In the case of intertube doping, 63% of the charge is given to the inner (5, 0) tube and the remaining 37% to the outer (14, 0) tube. In the case of exterior doping, most of the charge (80%) is donated to the outer (14, 0) tube as expected. It is interesting to find there is still a small fraction of the charge (21%) that are donated to the inner (5, 0) tube even it is a bit far away from the Li atom. Such long-distance charge transfer could be only realized via intertube interactions.

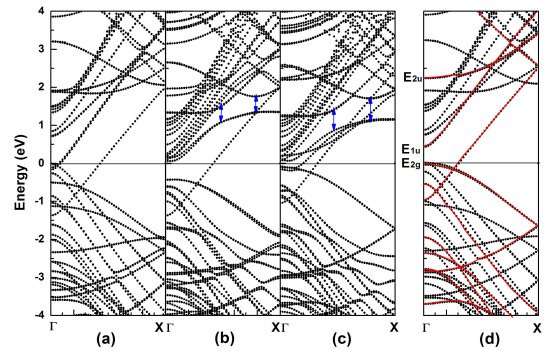


FIG. 13. Energy band structures of DCNT with Li doped at (a) site A, (b) site B, and (c) site C. Note the system has a concentration of  $C_{76}Li$ . For comparison, the band structure of un-doped DCNT is shown in (d) where the bands from (5, 0) tube are marked as red curves. The Fermi levels are at 0 eV. The blue arrows indicate obvious band-splitting

We now consider the high concentration limit of Li doping. As site B is the most favorable and there are many equivalent positions between the inner and outer tubes, it is anticipated that the Li atoms can be doped with a large amount. To get a high Li concentration,

TABLE V. Bader charge analysis for the charge transfer in the DCNT (5, 0)@(14, 0). The values (in unit of electrons) indicate the net charge received upon Li doping.

sites	inner (5, 0)	outer (14, 0)
A	0.962	0.038
B	0.634	0.366
C	0.207	0.793

14 Li atoms are introduced into the intertube space and arranged in two alternate layers. In each layer, there are 7 Li atoms which are initially positioned according to the symmetry of outer (14, 0) tube. The Li binding energy for such configuration is calculated to be  $-1.17$  eV which means that the doping is still favorable at such high concentration ( $C_{76}Li_{14}$ ). It is interesting to note that the concentration can be further increased if one more Li atom is inserted into the interior of (5, 0) tube and another is located outside the (14, 0) tubes. The obtained configuration thus contains 16 Li atoms per unit cell with nominal formula of  $C_{76}Li_{16}$  or  $LiC_{4.75}$ . This concentration corresponds to a Li intercalation capacity of 470 mAh/g, which is significantly higher than the upper limit of graphite intercalated compounds (372 mAh/g). We have examined the optimized structure of the DCNT with 16 Li atoms doped, and found there is only a slight deformation of tubes' structure compared with the un-doped case. The good structure stability together with the enhanced Li capacity suggests that (5, 0)@(14, 0) DCNT may have potential application in Li-ion battery. It would be interesting to experimentally test this prediction when (5, 0)@(14, 0) DWNT is formed by technique such as coalescence of small C20 molecule confined inside a larger (14, 0) tube.

## VI. SUMMARY

In summary, we show by first-principles calculations that the 4 Å carbon nanotubes and their related structures exhibit much higher Li intercalation capacity and could be very promising candidates for Li battery applications. It should be mentioned that carbon nanotubes observed in the experiments usually self-organize into a crystalline bundle where the tube-tube interactions play an very important role. Due to the large curvature, these ultrasmall nanotubes are expected to be more reactive than larger-diameter ones. For example, the (5, 0) tubes prefer to form a triplet bundle<sup>[42]</sup> by strong chemical bonds rather than the weak van der Waals interactions. The unique atomic configuration gives the (5, 0) triplet an ideal candidate for Li intercalation, which needs further experimental and theoretical investigations.

## ACKNOWLEDGMENTS

We thank Prof. C. T. Chan, Prof. P. Sheng, Prof. Z. K. Tang for many helpful discussions. This work was supported by the National Natural Science Foundation (Grant No. 10504025 and 51172167) and the Program for New Century Excellent Talents in University.

## REFERENCES

- [1] Iijima S. *Nature* (London), 1991, **354**: 56
- [2] Saito R, Dresselhaus G, Dresselhaus M S. *Physical Properties of Carbon Nanotubes*, 1998 (Imperial College Press, London)
- [3] Miyamoto Y, Rubio A, Blase X, Cohen M L, Louie S G. *Phys. Rev. Lett.*, 1995, **74**: 2993
- [4] Frackowiak E, Gautier S, Gaucher H, Bonnamy S, Beguin F. *Carbon*, 1999, **37**: 61
- [5] Gao B, Kleinhammes A, Tang X P, Bower C, Fleming L, Wu Y, Zhou O. *Chem. Phys. Lett.*, 1999, **307**: 153
- [6] Jouguelet E, Mathis C, Petit P. *Chem. Phys. Lett.*, 2000, **318**: 561
- [7] Zhao J J, Buldum A, Han J, Lu J P. *Phys. Rev. Lett.*, 2000, **85**: 1706
- [8] Tarascon J M, Armand M. *Nature* (London), 2001, **414**: 359
- [9] Ishihara T, Kawahara A, Nishiguchi H, Yoshio M, Takita Y. *J. Power Sources*, 2001, **97-98**: 129
- [10] Shimoda H, Gao B, Tang X P, Kleinhammes A, Fleming L, Wu Y, Zhou O. *Phys. Rev. Lett.*, 2001, **88**: 015502
- [11] Meunier V, Kephart J, Roland C, Bernholc J. *Phys. Rev. Lett.*, 2002, **88**: 075506
- [12] Wang G X, Ahn J, Yao J, Lindsay M, Liu H K, Dou S X. *J. Power Sources*, 2003, **119-121**: 16
- [13] Garau C, Frontera A, Quiñero D, Costa A, Ballester P, Deyà P M. *Chem. Phys. Lett.*, 2003, **374**: 548
- [14] Chen W X, Lee J Y, Liu Z L. *Carbon*, 2003, **41**: 959
- [15] Morris R S, Dixon B G, Gennett T, Raffaele R, Heben M J. *J. Power Sources*, 2004, **138**: 277
- [16] Larciprete R, Petaccia L, Lizzit S, Goldoni A. *Phys. Rev. B.*, 2005, **71**: 115435
- [17] Udomvech A, Kerdcharoen T, Osotchan T. *Chem. Phys. Lett.*, 2005, **406**: 161
- [18] Wang X H, Liu H W, Jin Y, Chen C H. *J. Phys. Chem. B*, 2006, **110**: 10236
- [19] Schmid M, Goze-Bac C, Kramer S, Roth S, Mehring M, Mathis C, Petit P. *Phys. Rev. B.*, 2006, **74**: 073416
- [20] Zhou Z, Zhao J J. *Prog. in Phys.*, 2007, **27**: 92
- [21] Khantha M, Cordero N A, Alonso J A, Cawkwell M, Girifalco L A. *Phys. Rev. B.*, 2008, **78**: 115430
- [22] Kaskhedikar N A, Maier J. *Adv. Mater.*, 2009, **21**: 2664
- [23] Wen Y W, Liu H J, Tan X J, Pan L, Shi J. *J. Appl. Phys.*, 2010, **107**: 034312
- [24] Wang N, Tang Z K, Li G D, Chen J S, *Nature* (London), 2000, **408**: 51
- [25] Li Z M, Tang Z K, Liu H J, Wang N, Chan C T, Saito R, Okada S, Li G D, Chen J S, Nagasawa N, Tsuda

- S. *Phys. Rev. Lett.* 2001, **87**: 127401
- [26] Liu H J, Chan C T. *Phys. Rev. B*, 2002, **66**: 115416
- [27] Kresse G, Hafner J. *Phys. Rev. B*, 1993, **47**: 558
- [28] Kresse G, Hafner J. *Phys. Rev. B*, 1994, **49**: 14251
- [29] Kresse G, Hafner J. *Comput. Mater. Sci.*, 1996, **6**: 15
- [30] Perdew J P, Wang Y. *Phys. Rev. B*, 1992, **45**: 13244
- [31] Yang J L, Liu H J, Chan C T. *Phys. Rev. B*, 2001, **64**: 085420
- [32] Qiu S, Pang W, Kessler H, Guth J L. *Zeolites*, 1989, **9**: 440
- [33] Liu H J, Li Z M, Liang Q, Tang Z K, Chan C T. *Appl. Phys. Lett.*, 2004, **84**: 2649
- [34] Hu Y, Liu H J, Miao L, Wen Y W, Shi J. *Microporous Mesoporous Mater.*, 2008, **116**: 233
- [35] Deiss E, Wokaun A, Barras J L, Daul C, Dufek P. *J. Electrochem. Soc.*, 1997, **144**: 11
- [36] Aydinol M K, Kohan A F, Ceder G, Cho K, Joannopoulos J. *Phys. Rev. B*, 1997, **56**: 1354
- [37] Courtney I A, Tse J S, Mao O, Hafner J, Dahn J R. *Phys. Rev. B*, 1998, **58**: 15583
- [38] Zólyomi V, Koltai J, Ruzsnyák Á, Kürti J, Gali Á, Simon F, Kuzmany H, Szabados Á, Surján P R. *Phys. Rev. B*, 2008, **77**: 245403
- [39] Henkelman G, Arnaldsson A, Jónsson H. *Comput. Mater. Sci.*, 2006, **36**: 254
- [40] Sanville E, Kenny S D, Smith R, Henkelman G. *J. Comp. Chem.*, 2007, **28**: 899
- [41] Tang W, Sanville E, Henkelman G. *J. Phys.: Condens. Matter*, 2009, **21**: 084204
- [42] Wen Y W, Liu H J, Pan L, Tan X J, Lv H Y, Shi J, Tang X F. *J. Phys. Chem. C*, 2011, **115**: 9227

## 4 Å 碳纳米管及相关结构的嵌锂特性

刘惠军

人工微结构教育部重点实验室、武汉大学物理科学与技术学院，武汉 430072

**摘要：**碳纳米管独特的一维结构和强烈的卷曲效应为外来原子提供了理想的嵌入通道。本文全面总结了近年来我们对直径仅为 4 Å 的三种单壁碳纳米管嵌锂特性的密度泛函研究工作。我们具体讨论了体系嵌锂后的结构、能量、电子、电化学等特性。由于这些超小直径的碳纳米管最初合成于沸石晶体的纳米管道，我们也讨论了碳纳米管-沸石晶体复合体系的嵌锂特性。另外，我们还研究了由 (5, 0) 和 (14, 0) 碳纳米管组成的双壁碳纳米管体系的嵌锂特性。我们的理论计算表明，超小直径碳纳米管及相关结构作为锂离子电池负极材料具有很好的应用前景。

**关键词：**碳纳米管；锂嵌入；锂离子电池；电子特性；电化学特性；密度泛函计算